The Journal of Chemical Physics ARTICLE scitation.org/journal/jcp

Comprehensive investigation on the triplet state electronic structure of free-base 5,10,15,20-tetrakis(4-sulfonatophenyl) porphyrin by a combined advanced EPR and theoretical approach

Cite as: J. Chem. Phys. 152, 000000 (2020); doi: 10.1063/1.5131753
Submitted: 15 October 2019 • Accepted: 19 December 2019 •
Published Online: XX XX XXXX

View Online Export Citation CrossMark

Antonio Barbon,[a] Maria Giulia Dal Farra,[a] Susanna Ciuti, Marco Albertini, Luca Bolzonello, Laura Orian,[b] and Marilena Di Valentin[c]

AFFILIATIONS

Dipartimento di Scienze Chimiche, Università degli Studi di Padova, Via Marzolo 1, 35131 Padova, Italy

Note: This paper is part of the JCP Special Topic on Spin Chemistry.
[a]**Contributions:** A. Barbon and M. G. D. Farra contributed equally to this work.
[b]**E-mail:** laura.orian@unipd.it
[c]**E-mail:** marilena.divalentin@unipd.it

ABSTRACT

The nature of the photoexcited triplet state of free-base 5,10,15,20-tetrakis(4-sulfonatophenyl)porphyrin (H_2TPPS^{4-}) has been investigated by advanced Electron Paramagnetic Resonance (EPR) techniques combined with quantum chemical calculations. The zero-field splitting (ZFS) parameters, D and E, the orientation of the transition dipole moment in the ZFS tensor frame, and the proton hyperfine couplings have been determined by magnetophotoselection-EPR and pulse electron-nuclear double resonance spectroscopy. Both time-resolved and pulse experiments exploit the electron spin polarization of the photoexcited triplet state. Comparison of the magnetic observables with computational results, including CASSCF calculations of the ZFS interaction tensor, provides an accurate picture of the triplet-state electronic structure. The theoretical investigation has been integrated with a systematic analysis on the parent free-base porphyrin molecule to assess the effect of the sulfonatophenyl substituents on the magnetic tensors. Additionally, the magnetophotoselection effects are discussed in terms of tautomerization in the excited singlet state of H_2TPPS^{4-}.

Published under license by AIP Publishing. https://doi.org/10.1063/1.5131753

I. INTRODUCTION

Porphyrins and their derivatives constitute an important class of biomolecules because of their involvement in several fundamental biochemical processes.[1,2] To date, the main application of these compounds has been as model biosystems and, interestingly, also in the field of applied sciences. Porphyrin-based materials are good candidates for molecular electronic devices, new solar cells, and they have been shown to function as components of molecular and photonic wires and in nonlinear optical materials, to give only few significant examples.[3–7]

Among the properties that have received much attention in recent years, there is the ability of porphyrinoid molecules to participate in energy-transfer and electron-transfer reactions, playing a central role in these photoinitiated processes in a similar manner as chlorophyll and bacteriochlorophylls act in the primary events of photosynthesis.[8,9] Inspired by natural photosynthetic antenna complexes and reaction centers, porphyrin-based systems are being designed and investigated for applications in artificial photochemical conversion and storage of solar energy.[10,11] Water-soluble porphyrins are considered particularly suited for such applications. Among selfassembling chromophores, they are gaining a relevant

Author Proof

Published under license by AIP Publishing

position as building blocks for the design of chlorosome-mimicking antennas due to the possibility of fine-tuning of their spectroscopic and structural properties by conveniently modifying their sidechains.[12,13] A smart technique to control the aggregation process of tetraphenylporphyrin derivatives involves functionalization of the side chains with charged groups and the fine regulation of the pH of the solvent,[14,15] as in the case of the anionic free-base 5,10,15,20-tetrakis(4-sulfonatophenyl)porphyrin ($\mathbf{H_2TPPS^{4-}}$), which forms J-aggregates in acidic aqueous solutions.[16–18]

Determining the extent to which the $\mathbf{H_2TPPS^{4-}}$ moiety may or may not be effective as a model compound in artificial photosynthesis requires a detailed understanding, and hence an extensive characterization, of its photophysical properties in terms of excited states. While the singlet excited states have been thoroughly investigated also from the computational point of view, less is known about the triplet state due to the *dark* nature of this state that precludes the application of most of the optical spectroscopies. Photogenerated triplets are key reaction intermediates in many light-induced processes and they show encouraging features that can be exploited in the field of solar light harvesting.[19]

A time-resolved Electron Paramagnetic Resonance (TR-EPR) investigation[20] on the triplet state of $\mathbf{H_2TPPS^{4-}}$ in different monomeric and aggregated forms has shown variations in the magnetic properties going from one species to the other, which have prompted us to further investigate the free-base $\mathbf{H_2TPPS^{4-}}$ (the molecular structure is shown in Fig. 1) by advanced magnetic resonance and theoretical methodologies.

TR-EPR is a powerful technique for the investigation of photoexcited triplet states and extensive studies employing this spectroscopy have been performed on porphyrins.[21,22] The key data are the zero-field splitting (ZFS) parameters D and E, which are sensitive indicators of the spatial extension and symmetry of the two singly occupied molecular orbitals of the triplet state. In addition, TR-EPR allows us to determine the orientation of this interaction within the molecule, probing the geometrical relation between the optical transition dipole moment (TDM) of the molecule and the

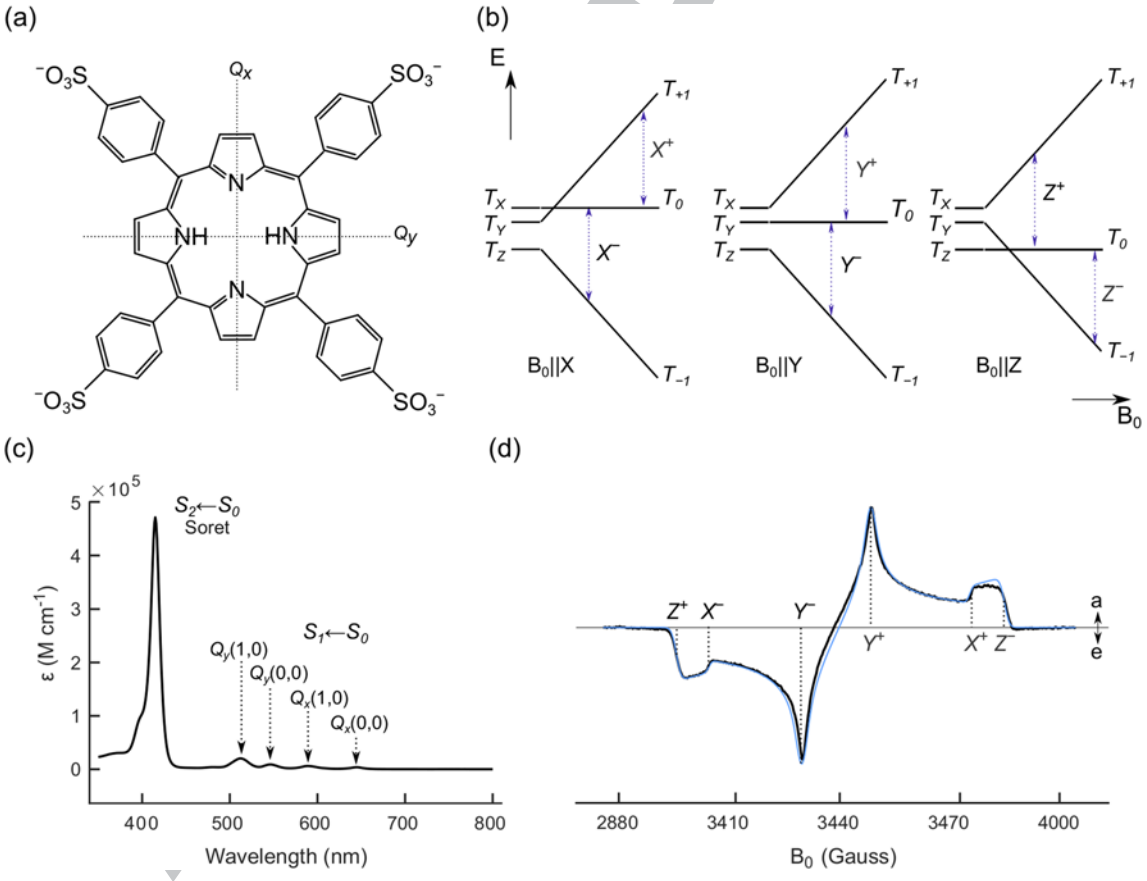

FIG. 1. (a) Molecular structure of $\mathbf{H_2TPPS^{4-}}$ with the corresponding TDM directions for the Q_x and Q_y transitions. (b) Energy diagram of the triplet spin sublevels, for $D > 0$ and $E < 0$, as a function of the magnetic field B_0, with the field vector parallel to the principal axes of ZFS. The arrows indicate the allowed EPR transitions according to the selection rule $\Delta m_S = \pm 1$. (c) Room-temperature absorption spectrum of $\mathbf{H_2TPPS^{4-}}$ in ethanol/methanol 3:2 solution, with the names of the absorption bands according to the Gouterman model.[64] (d) Isotropically excited TR-EPR spectrum of $\mathbf{H_2TPPS^{4-}}$ (black) and corresponding simulation (light blue). The simulation parameters are reported in Table I.

Published under license by AIP Publishing

resulting triplet state by using linearly polarized light for excitation.[21,23,24] In the past, such magnetophotoselection experiments were performed on aromatic molecules and were crucial in revealing details of the electronic structure of the main chromophores taking part in early events of photosynthesis.[25,26] Magnetophotoselection has been recently reproposed to study porphyrin model compounds.[27,28]

The ZFS parameters are integral properties of the triplet wavefunction and depend on its overall spatial distribution. More specific information about the electron distribution in the HOMO and LUMO orbitals is obtained from the electron-nuclear hyperfine coupling (hfc) tensors, from which the distribution of the unpaired electrons of the triplet state is obtained.[22,29] In contrast to the large body of EPR and Optically Detected Magnetic Resonance investigations yielding D and E parameters and, in the case of TR-EPR, also the electron spin-polarization pattern, there are only a few studies on the hyperfine structure of the triplet state of porphyrins resolved by Electron-Nuclear Double Resonance (ENDOR) spectroscopy.[27,30–33] Pulse ENDOR, combined with repetitive laser excitation, takes advantage of the large spin polarization of the triplet state being present only in the first few microseconds after the laser pulse.

Detailed information on the structure of the porphyrin triplet state may be derived by comparison of experimental ZFS parameters and proton hfc values (hfcs) with the results of quantum mechanical calculations. Nowadays, computational methods are well established for most of the spin Hamiltonian parameters, such as hfc tensors and g tensors.[34] The additional fine structure observed in triplet state spectra due to the electron–electron spin coupling, in contrast to the other spin Hamiltonian terms, has been addressed only for small molecules and there is not a consolidated approach for its quantitative analysis.[35–37] A limited number of theoretical studies undertaking the calculation of the ZFS tensor of porphyrins has been reported so far and, to the best of our knowledge, no one based on multiconfiguration post HF methods for this important class of heterocyclic tetrapyrrolic compounds.[27,38,39]

In this contribution, a comprehensive study of the triplet state of $\mathbf{H_2TPPS^{4-}}$ is provided by combining the advanced EPR techniques, best-suited for the triplet state investigation, and state-of-the-art computational methods, which permit accurate calculation of the magnetic observables, i.e., ZFS parameters and proton hfcs. In parallel, the free-base porphyrin ($\mathbf{H_2P}$) molecule, which is the parent compound, will be addressed to stress the similarities and differences due to the substituents in $\mathbf{H_2TPPS^{4-}}$. The nice agreement between the experimental and computed hfcs and ZFS parameters, including the ZFS tensor orientation with respect to the TDM, allows us to propose a reliable and detailed picture of the triplet wavefunction of a representative member of this important class of molecules. This is essential for designing novel artificial systems and for developing further applications, which exploit the photophysics of the triplet state.

II. MATERIALS AND METHODS

A. Sample preparation

$\mathbf{H_2TPPS^{4-}}$ was purchased from Sigma Aldrich and used without further purification. All the $\mathbf{H_2TPPS^{4-}}$ solutions used for spectroscopic characterization were freshly prepared by dissolving the powder in a mixture of ethanol and methanol 3:2. The concentration of the solutions was determined by optical absorption spectroscopy and has a final value of about 60 μM. The choice of using a mixture of ethanol and methanol for the monomeric samples has the important advantage of generating a good glass when frozen.

Samples for EPR were degassed by freeze and thaw cycles, inserted into quartz EPR tubes (2.4 mm inner diameter, 4 mm outer diameter), sealed under vacuum, and immediately frozen in liquid nitrogen. Samples were stored in liquid nitrogen until measurements.

B. EPR measurements

TR-EPR spectra were recorded at X-band on a Bruker Elexsys E580 spectrometer equipped with a dielectric cavity thermostated at 80 K with a cold nitrogen vapor flow inside a CF935 cryostat. The microwave power used for the TR-EPR experiments was about 1.5 mW. TR-EPR spectra were recorded in direct detection mode without applying any field modulation or phase-sensitive detection. The EPR signals were collected from the microwave preamplifier (bandwidth 20 Hz–6.5 MHz) and sampled with a LeCroy 9360 oscilloscope (10 ns per point). The time resolution of the spectrometer has been estimated to be about 900 ns, mainly due to the cavity response. Laser excitation of the samples was performed using an optical parametric oscillator (OPO) pumped by the third harmonic of a Nd:YAG laser (Quantel Rainbow), operating at a repetition rate of 10 Hz. Laser pulses were 5 ns long, with energies of 3.5 mJ, and a wavelength of 520 nm. Two different polarizations of the light were employed for the magnetophotoselection experiments: one with the electric field perpendicular and the other parallel to the static magnetic field of the spectrometer. The rotation of the polarization plane of the light was obtained using a half waveplate; a linear polarizer was added near the optical window of the cavity for a better control of the polarization. To record the isotropic TR-EPR spectrum, a solution frozen to form a bad milky glass (therefore composed of microcrystallites) was used in order to obtain depolarization by multiple scattering events.

X-band pulse EPR experiments were conducted on a Bruker Elexsys E580 equipped with a dielectric ENDOR cavity (EN4118X-MD4) ~9.5 GHz. The temperature was maintained at 20 K with a helium cryostat with optical access (Oxford CF935) driven by a temperature controller (Oxford ITC503). The radio frequency (RF) amplifier was ENI A-500W. Pulsed laser excitation at 532 nm (5 mJ per pulse and repetition rate of 10 Hz) was provided by the second harmonic of a Nd:YAG laser (Quantel Brilliant). Field-swept electron spin echo spectra were recorded using a two-pulse echo sequence according to the scheme: flash–DAF–$\pi/2$–τ–π–τ–echo (DAF = delay after flash). Mims ENDOR experiments were recorded using the microwave pulse sequence, flash–DAF–$\pi/2$–τ–$\pi/2$–T–$\pi/2$–echo, with 16 ns pulse duration, in conjunction with an RF pulse of 6 μs duration located during the delay T and starting 1.2 μs after the second microwave pulse. The delay τ was variable and the time T was 8.8 μs, long enough to accommodate the RF pulse. Mims ENDOR spectra were recorded at three different τ values (120, 180, and 240 ns) and added together to eliminate τ-dependent blind spots. Pulse ENDOR spectra were accumulated for ~5 h.

Author Proof

Published under license by AIP Publishing

C. Spectral analysis

TR-EPR data were processed by subtracting: (i) the average baseline before the trigger event and (ii) a time profile taken at an off-resonance position. Spectra were extracted as single time points at about 1.4 μs after pulsed laser excitation.

Simulations of triplet spectra have been performed using a home-written MATLAB program. For the isotropically excited TR-EPR spectrum, the parameters of the simulations include the g and ZFS tensors and the relative triplet sublevel populations. For the magnetophotoselection TR-EPR spectra, in order to take into account the photoselection of specific orientations, a probability function is also included.

TR-EPR spectra recorded for light polarized parallel and perpendicular to the magnetic field direction were analyzed according to Ref. 23. Here, only a brief summary of the procedure is presented.

When a polarized light source is used to photoexcite the sample, the probability to excite each molecule depends on the angle between the TDM and the direction of the light polarization. Assuming that, after the light excitation, an efficient intersystem crossing (ISC) takes place, the orientational distribution of triplet states inside the sample is uneven and depends on the direction of the TDM in the ZFS reference frame. For the analysis of the TR-EPR spectra in the presence of magnetophotoselection, it is convenient to express the probability p of exciting a specific molecular orientation as a function of the three Euler angles, (α, β, γ), between the laboratory frame and the ZFS axes. For a specific orientation of the TDM in the ZFS frame, defined by the angles ω, φ, the excitation probability is

$$p_{\omega,\varphi}^{\mathrm{par/perp}}(\alpha,\beta,\gamma) = (\hat{\boldsymbol{u}}_{TDM}\cdot\hat{\boldsymbol{u}}_{E})^{2}/N, \tag{1}$$

where $\hat{\boldsymbol{u}}_{TDM}$ and $\hat{\boldsymbol{u}}_{E}$ are the unit vectors along the direction of the TDM and the electric field component of the light. This probability function takes into account that molecules with different orientations are excited when the polarization of the light is varied from a parallel to a perpendicular configuration with respect to the static magnetic field.

The spectrum is calculated as[40]

$$I(B_0)^{\mathrm{par/perp}} = \sum\nolimits_{+/-}\int_0^{2\pi}\int_0^{\pi} G[B_{\mathrm{res}}(\alpha,\beta)-B_0] \cdot P_{\pm}(\alpha,\beta,B_0)\cdot\left[\int_0^{2\pi} p_{\omega,\varphi}^{\mathrm{par/perp}}(\alpha,\beta,\gamma)d\gamma\right]\sin\beta d\alpha d\beta, \tag{2}$$

where $G[B_{\mathrm{res}}(\alpha,\beta)-B_0]$ is a Gaussian line shape function centered at the resonance field B_{res}, $P_{\pm}(\alpha,\beta,\gamma)$ is the non-Boltzmann population difference between the two resonant states, and $p_{\omega,\varphi}^{\mathrm{par/perp}}(\alpha,\beta,\gamma)$ is the excitation probability specific for the parallel and perpendicular configuration. The analytical expressions obtained for the integral within the square brackets for the two orientations of the light polarization with respect to the static magnetic field are reported in the supplementary material.

In the simulation of the magnetophotoselection data, depolarization effects are taken into account by allowing a low-weight contribution from isotropic light excitation. These effects are mainly due to multiple reflections inside the cavity and scattering of the light.

For the Mims ENDOR experiments, the values of the proton hfcs along the principal axes of the ZFS tensor were determined by Gaussian deconvolution of the ENDOR spectra.

D. Computational details

All calculations were carried out with the Amsterdam Density Functional (ADF) suite of programs.[41–43] The hybrid B3LYP functional was used[44–46] combined with a triple-ζ quality basis set of Slater-type functions (TZ2P) augmented with two sets of polarization functions. The innermost orbitals of each element were kept constant during the SCF cycles (frozen core approximation): up to 1s for carbon, nitrogen, oxygen, and sulfur. Dispersion effects were included using the correction proposed by Grimme, i.e., D3 with a BJ damping function.[47] This level of theory is denoted B3LYP-D3(BJ)/TZ2P. First, geometry optimizations of the archetypal **H$_2$P** and of **H$_2$TPPS^{4-}** were performed using D_{2h} symmetry constraint.

TD-DFT calculations were carried out on the optimized geometries using all-electron TZ2P basis sets for all the atoms. The approximate xc potential obtained with the statistical averaging of (model) orbital potentials (SAOP) was used to calculate the excitation energies, which is suitably designed with a correct asymptotic behavior[48,49] and has been employed with success to investigate excited state properties.[50–52]

For the calculation of the hyperfine tensor, zero field splitting tensor, and spin density, both B3LYP-D3(BJ) and BP86[53–55] functionals were used combined with all-electron TZ2P basis set. The scalar zeroth order regular approximation (ZORA)[56–58] was employed to account for relativistic effects. These levels of theory are denoted ZORA-B3LYP-D3(BJ)/TZ2Pae and ZORA-BP86/TZ2Pae, respectively. No appreciable differences were found and so only data computed at the former level of theory will be discussed in the text. In order to investigate the effect of different orientations of the phenyl rings, geometries were manually built starting from the D_{2h} optimized structures with the rings at 30° and 60° with respect to the tetrapyrrolic plane, without altering the porphyrin core. In addition, for these dihedral values (which are explained in detail in Fig. S9), different mutual orientations of the rings were considered. The magnetic observables were computed for these geometries at the ZORA-BP86/TZ2Pae level of theory.

Due to the unsatisfactory results for the D tensor, ascribed mainly to the limitations of the single-determinant DFT approach, CASSCF calculations were carried out to compute the zero field splitting tensor, as implemented in ORCA software package.[59] The structures obtained by D_{2h} constrained geometry optimizations at the B3LYP-D3(BJ)/TZ2P level were used. MP2 natural orbitals from the unrelaxed density matrix were generated and employed as starting guess. The def2-TZVP basis set was used for all the atoms and def2-TZVP/C was used for the RI approximation. In the CASSCF calculations, def2/J in conjunction with RIJCOSX was employed to approximate the Fock operator for **H$_2$TPPS^{4-}**. A CAS(4,4) active space was chosen including the two π and the two π* frontier molecular orbitals of **H$_2$P** and **H$_2$TPPS^{4-}**. The sets of four MP2 natural orbitals are shown in Figs. S1 and S2. The spin orbit contribution to the D tensor was computed, but, as expected, it resulted to be negligible; thus, the values reported and discussed in the text correspond to the spin-spin contribution.

Author Proof

Published under license by AIP Publishing

III. RESULTS

A. Time-resolved EPR and magnetophotoselection

Magnetophotoselection is a phenomenon observed for photoexcited triplet states, generated by light polarized parallel or perpendicular to the magnetic field, making the relative intensities of the EPR lines dependent on the light polarization. It is a consequence of the fact that the EPR intensities depend not only on the population difference between the triplet sublevels, but also on the nonuniform spatial distribution of the molecules due to selective excitation. Magnetophotoselection has been used in a limited number of cases to attain quantitative information on the relative orientation of the ZFS tensor axes with respect to the optical transition moment, if one of the two is known.[23,60,61]

For $\mathbf{H_2TPPS^{4-}}$, having a D_{2h} symmetry, the two absorption Q bands are not degenerate and this results in two resolved sets of peaks exhibiting a vibronic structure,[62] with both the 0–0 and the 0–1 transitions visible in the absorption spectrum as shown in Fig. 1(c). The Q_y and Q_x transitions are characterized by a TDM aligned along and perpendicular to the NH bonds, respectively, as reported in the literature[63] and confirmed by the present DFT calculations (see Table S2 in the supplementary material). This configuration is opposite to the one reported for $\mathbf{H_2P}$.[63] The overall set of optical properties calculated for $\mathbf{H_2TPPS^{4-}}$ is summarized in the supplementary material as they are functional to the calculations of the magnetic properties derived from EPR-magnetophotoselection. The magnetophotoselection experiments were performed by exciting the Q_y transition by irradiating at 520 nm, where both the Q_x transition and the J-aggregates have negligible absorption.[20]

At first, the isotropically excited TR-EPR spectrum was obtained from the frozen solution of $\mathbf{H_2TPPS^{4-}}$ (see the experimental details in the Materials and Methods section and Fig. S7). Then, the TR-EPR spectra recorded after excitation of $\mathbf{H_2TPPS^{4-}}$, in a transparent glass carefully prepared to avoid cracks, with light polarized parallel and perpendicular to the magnetic field, were obtained and they are shown in Fig. 2. Since the experimental set-up assured the same excitation conditions, the spectra are displayed without renormalization and show an evident magnetophotoselection effect, with enhanced X and Y triplet transitions in the parallel spectrum and enhanced Z transitions in the perpendicular spectrum. The spectra are also different from that obtained by isotropic irradiation. To further confirm isotropic excitation of the molecules, we have compared the spectrum lineshape obtained with isotropic irradiation with the one calculated as the sum of the experimental spectrum recorded after excitation with polarization of the light parallel to the external magnetic field and twice the spectrum obtained with perpendicular polarization, in analogy to optical polarization measurements.[65] A nice matching of the lineshape of

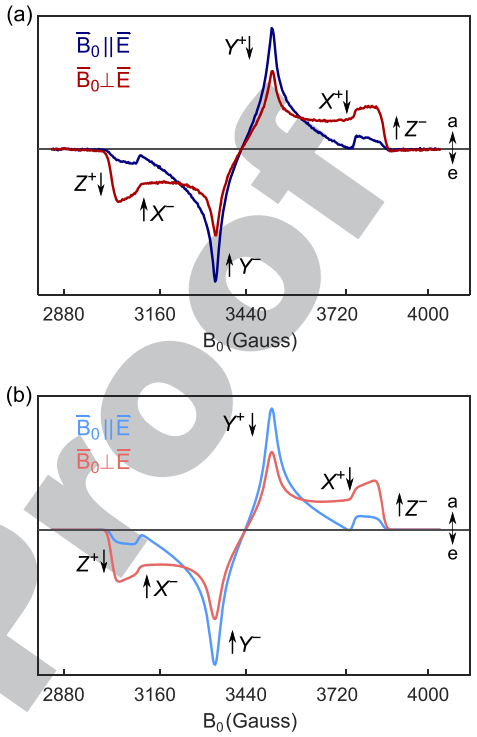

FIG. 2. (a) TR-EPR spectra of $\mathbf{H_2TPPS^{4-}}$, recorded at 80 K, using an excitation light polarized parallel (blue) and perpendicular (red) to the magnetic field. (b) Simulations of the TR-EPR spectra of $\mathbf{H_2TPPS^{4-}}$ with polarization of the light parallel (light blue) and perpendicular (light red) to the magnetic field. The simulation parameters are reported in Table I. The black arrows represent the enhancement or the reduction of the signal when going from parallel to perpendicular excitation at the canonical positions.

TABLE I. ZFS parameters, relative triplet sublevel populations, and TDM orientation in the ZFS axes system determined through simulation of the TR-EPR spectra.

	$D(10^{-4}\ \mathrm{cm}^{-1})$	$E(10^{-4}\ \mathrm{cm}^{-1})$	p_x	p_y	p_z	ω (deg)	φ (deg)	Weight (%)
Simulation[a]	391	−76	0.3	0.6	0.1	90	0	50
						90	90	50
Computation[b]	208	5	...	...	...	...	...	...

[a]The D and E parameters and p_x, p_y, p_z were obtained from simulation of the isotropically excited TR-EPR spectrum. ω, φ, and weight were extracted from simulation of the TR-EPR spectra recorded in the magnetophotoselection experiments. ω is the angle between the Z axis of the ZFS axes system and the TDM, and φ is the angle between the X axis of the ZFS axes system and the TDM projection into the XY plane (see Fig. 2). Weight is the contribution of each set of angles to the simulation.
[b]Level of theory: CASSCF(4,4)/def2-TZVP//B3LYP-D3(BJ)/TZ2P.

Author Proof

Published under license by AIP Publishing

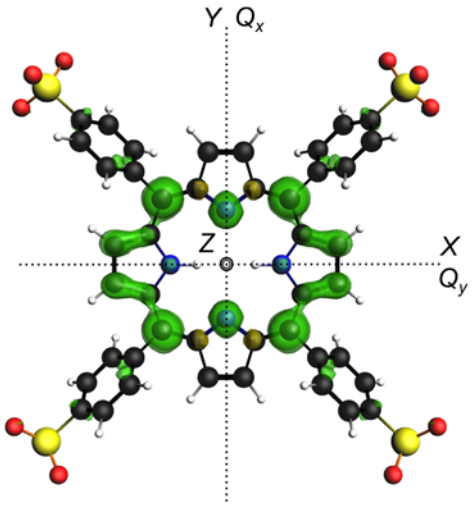

FIG. 3. Optimized geometry of H_2TPPS^{4-} [level of theory: B3LYP-D3(BJ)/TZ2P] and triplet state spin density [level of theory: BP86/TX2Pae//B3LYP-D3(BJ)/TZ2P] with the calculated orientations of the optical TDM and the ZFS principal axes [level of theory: CASSCF(4,4)/def2-TZVP//B3LYP-D3LYP(BJ)TZ2P].

the experimental and the calculated spectra was obtained, as shown in Fig. S7.

Spectral simulations were performed in order to define quantitatively the geometrical relation between the TDM and the ZFS tensor axes in the magnetophotoselection experiments. The key parameter of the simulation is the orientational distribution function reported in Eq. (1), while D, E, and the relative triplet population rates are fixed parameters and are derived from the isotropically excited spectrum. The simulations exhibit not only the correct lineshape, but also the experimental trend in terms of relative intensities. Unexpectedly, the outcome of the global fitting is that the distribution function is the sum of two contributions, with either the principal axes X and Y of the ZFS system aligned along the TDM with an equal weight and an estimated error of 5° at most (for details see Fig. S8 in the supplementary material). A single contribution is unable to reproduce all the features of the spectra and the intensity variations from the parallel to the perpendicular configuration. No optical TDM is associated with the triplet Z axis, confirming the assignment of this axis to the out-of-plane direction and the positive value of D for H_2TPPS^{4-} as found for other free-base analogs.[66] Table I summarizes the outcome of the spectral analysis, comparing the results on the ZFS tensor with those calculated using the CASSCF method. The orientation of the ZFS tensor in the molecular frame, as derived from computations, is displayed on top of the optimized geometry of H_2TPPS^{4-} in Fig. 3.

B. Triplet state ^{1}H ENDOR

Triplet state ^{1}H ENDOR permits measurement of the hfc tensor component in the reference frame of the ZFS tensor, since it is characterized by a strong orientation selection. For each EPR canonical transition, there are two ENDOR resonance frequencies at

$$\nu_{ENDOR}(0) = \nu_H, \tag{3}$$

$$\nu_{ENDOR}(\pm 1) = \nu_H \pm A_i, \quad \text{with } i = X, Y, Z, \tag{4}$$

where ν_H is the free-proton nuclear Larmor frequency, A_i is the sum of the Fermi-contact interaction, A_{iso}, and the dipolar contribution.[21,67]

It can be seen from these equations that the resulting triplet-state ENDOR spectrum is asymmetric, providing the further advantage of allowing us to determine the sign of the hfcs relative to the sign of the D value. The line at resonance frequency ν_H is common for all protons and, consequently, attains a high intensity.

The ^{1}H Mims ENDOR spectra recorded for H_2TPPS^{4-} at two of the canonical field positions, Y^+ and Z^+, in protonated and deuterated solvent, are shown in Figs. 4(a) and 4(b). In the corresponding insets, the echo-detected spectrum is reported in order to highlight the working field positions. Since the D value for H_2TPPS^{4-} is known to be positive from CASSCF calculations, the sign of the proton hfcs is assigned as indicated on top of the ENDOR spectra. The hfcs along the Y and Z axes of the ZFS tensor were determined through Gaussian deconvolution, and the results are shown in Table II. The spectral features, which disappear in the spectra of D_2TPPS^{4-} in the deuterated solvent, are unambiguously assigned to the NH protons (3) since deuterium exchange takes place for those central protons.

A comparison with the results of the DFT calculations at the ZORA-BP86/YZ2Pae//B3LYP-D3(BJ)/TZ2P level on the excited triplet state of H_2TPPS^{4-} has allowed assignment of all the hfcs to specific protons. The calculations were performed in the ZFS tensor frame, as the principal hfc tensor components are, in most cases, not collinear with the ZFS tensor. The hfcs have been calculated for several different conformers with imposed rotations of the phenyl rings, as shown in Fig. S9. The calculated hfc tensors, reported in Table II, refer to the conformer, in which the phenyl rings have been rotated, counterclockwise-clockwise-clockwise-counterclockwise, by 60° with respect to the tetrapyrrolic plane. The choice of a specific conformer has been guided by the matching between the calculated and experimental hfcs. However, it has emerged from the analysis that, while the angle between the tetrapyrrole macrocycle and the phenyl substituents is affecting the hfcs significantly, the mutual orientation of the rings is not relevant. The conformation with the phenyl rings at 90° with respect to the tetrapyrrolic plane shows a number of ENDOR peaks smaller than that experimentally observed. Finally, the conformers with the rings at 30°, beyond being unstable from an energetic point of view, present strong deviations from the experimental hfcs in the Z components of H (4).[68] The results for all the conformations are summarized in Table S5 and the comparison between the experimental and calculated hfcs is reported in Fig. S10.

DFT calculations predict a single hfc for the H (1) and H (2) protons, while experimentally two hfcs can be attributed to the H (1) protons. This can be clearly seen in the ENDOR spectra corresponding to the Z transition and for this reason the deconvolution of the corresponding peaks requires a large Gaussian component or even two components. In the literature, the symmetry lowering from D_{2h} to C_{2h} was ascribed to interactions with the solvent or to the admixture of a second triplet state.[32,69]

The trend of the computed A_Z components is in excellent agreement with those determined experimentally: the α-protons H (2) have small negative hfcs, while the H (1) and the NH (3) have

Author Proof

Published under license by AIP Publishing

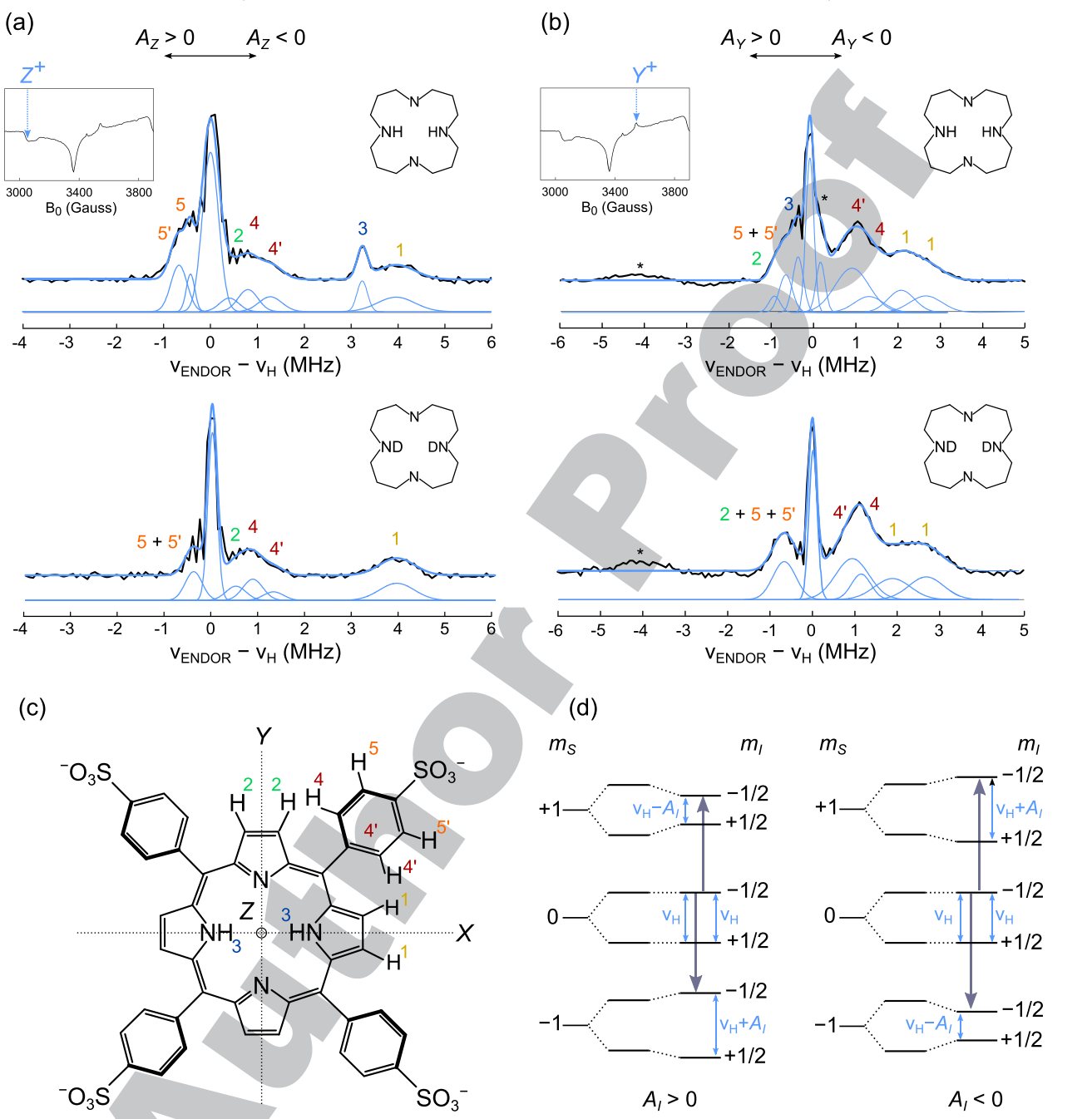

FIG. 4. X-band pulsed Mims ENDOR spectra of $\mathbf{H_2TPPS^{4-}}$ (top) and $\mathbf{D_2TPPS^{4-}}$ (bottom) recorded at 20 K along the Z^+ (a) and the Y^+ (b) ZFS canonical transitions, as indicated by the red arrows in the field-swept electron spin echo spectra shown in the insets. The ENDOR spectra are displayed together with the best fit (light blue) given by Gaussian functions below the spectra. The signs of the hfcs are shown above the spectra. The attribution of the peaks in the ENDOR spectra is represented according to the numbering scheme shown in (c). The asterisks denote the ENDOR peak arising from residual contributions of other orientations or free-proton lines disappearing after deuteration. (c) Molecular structure of $\mathbf{H_2TPPS^{4-}}$ and corresponding orientation of the ZFS principal axes and numbering scheme of the protons adopted in this work. (d) Energy of the spin sublevels of a triplet state coupled to a nucleus $I = 1/2$ with positive and negative hyperfine splitting, for the magnetic field parallel to a generic ZFS axis. The gray arrows indicate the EPR transitions for $m_I = -1/2$ (those for $m_I = +1/2$ are omitted), the light blue arrows indicate the ENDOR transitions.

Author Proof

Published under license by AIP Publishing

TABLE II. Experimental and computed proton hfc tensors of H_2TPPS^{4-} in the ZFS frame.

Hyperfine coupling (MHz)		H (1)[a]	H (2)	H (4)	H (4)′	H (5)	H (5)′	NH (3)[b]
ENDOR[c]	A_X	...	...	...	...	...	...	...
	A_Y	−2.17/−2.75	+0.84	−1.40	−1.00	+0.57	+0.57	+0.28
		−1.86/−2.69	+0.67	−1.15	−0.94	+0.67	+0.67	
	A_Z	−3.96	−0.40	−0.80	−1.28	+0.43	+0.67	−3.24
		−3.93	−0.50	−0.86	−1.30	+0.40	+0.40	
	A_{iso}	...	...	...	...	...	...	...
DFT	A_X	−1.81	+0.25	−0.69	−1.15	+0.81	+0.58	−0.08
	A_Y	−3.73	+1.03	−0.84	−0.60	+0.74	+0.80	−0.09
	A_Z	−3.79	−0.50	−0.75	−0.97	+0.66	+0.68	−3.08
	A_{iso}	−3.11	+0.26	−0.76	−0.91	+0.73	+0.69	−1.09

[a]Two values are reported for the A_Y component of H (1), because its ENDOR signal has been deconvoluted employing two Gaussian functions.
[b]The only hyperfine coupling available for the NH proton is that of the protonated porphyrin H_2TPPS^{4-}.
[c]For each proton, two experimental hfc values are reported: one for the fully protonated porphyrin, H_2TPPS^{4-} (top value), and the other for D_2TPPS^{4-} (bottom value).

larger negative hfcs. A similar behavior has been observed previously for both the H_2P and the free-base tetraphenylporphyrin molecules, indicating that the presence of the $(SO_3)^-$ substituent does not significantly affect the spin density distribution in the triplet state.[32] The small hfcs, in the vicinity of the strong Larmor peak, have been assigned to the different types of phenyl protons. Close to ν_H, there is also a contribution from protons with weak dipolar interactions with the unpaired electrons, such as protons in the solvent, which give rise to the "matrix" ENDOR line. These peaks disappear, as expected, in deuterated solvent.

The assignment of the experimental values obtained for A_Y, which has been reported in the literature only in the case of H_2P and for an incomplete set of protons,[70] is not as straightforward as for the A_Z components. Although the hfc calculated in the Y direction of the ZFS tensor is slightly overestimated for protons (1), even considering different possible conformers, the overall picture of the hfcs is perfectly in line with the experimental results. Small positive values are computed for the both the α-protons H (2) and the NH (3), while a larger negative contribution is found for the α-protons H (1).

Experimentally, the directions of the in-plane principal axes could not be distinguished by magnetophotoselection, as already pointed out in Sec. III A. Furthermore, although CASSCF calculations were performed to improve the accuracy of the ZFS parameters, E remains a critical parameter to be computed as it derives from the difference between two large components of the dipole–dipole coupling tensor. A significant inaccuracy in the estimation of E is accompanied by a potential mismatch of the directions of the associated in-plane principal axes. Indeed, a satisfactory agreement can also be obtained when comparing the ENDOR experimental values with the calculated A_X components, improving the accordance for protons (1) but at the expense of protons (2). This uncertainty is exacerbated by the impossibility to use the ENDOR data recorded along the X field position for an unequivocal assignment, due to the contamination of residual lines from other orientations. In addition, the orientation selection at the Y field positions is not as good as for the Z position, and therefore, hfcs are not as reliable.

From the assigned hfcs, a map of the spin-density distribution of the triplet electrons over the molecule can be obtained. The calculated spin-density plot is depicted in Fig. 3.

IV. DISCUSSION AND CONCLUSIONS

In this work, we elucidate the electronic structure of the lowest excited triplet state of H_2TPPS^{4-}. The interpretation requires a combination of magnetic resonance and accurate quantum chemistry methods in order to yield precious information on the triplet wavefunction. This is essential if a deeper understanding of the nature of this excited state has to be attained.

The approach here adopted is the combination of multiple EPR spectroscopic observables and computational results. The experiments allowed both ZFS and hfc tensors to be determined, the former with respect to the TDM in the magnetophotoselection experiment and the latter in the ZFS frame using pulsed ENDOR spectroscopy, as presented in the Results section. The existing literature on the EPR of the triplet state of porphyrins is complete in terms of ZFS parameters and spin polarization pattern but few EPR-magnetophotoselection experiments are available and no simulations are reported, allowing only a qualitative interpretation of the spectra, which contain important structural information.[27,71,72] For triplet states, in general, due to technical difficulties of performing ENDOR on transient species, only sparse experimental data have been reported on molecules of biological interest, including porphyrinoids.[21,22,32,73] In most cases, including the H_2P triplet state, only the A_Z component of the hfc tensor has been measured.[30,32] This prompted us to perform this comprehensive investigation. The interest for H_2TPPS^{4-} derives from the relevant applications of water-soluble porphyrins due to their ability to form J-aggregates. The accuracy in the study of porphyrin monomers appears as an important prerequisite for their use in aggregates.

The computational investigation on the electronic and magnetic features of the lowest excited triplet state of H_2TPPS^{4-} was preceded by a systematic analysis on the parent H_2P, which is the basic building block of the porphyrins, to assess the role of the

Author Proof

Published under license by AIP Publishing

substituents on the magnetic tensors, while the electronic absorptions have been more extensively discussed in the literature, as commented in the following.

For ^{1}**H$_2$P**, the four-level Gouterman model works well, since the frontier orbitals consist of two almost degenerate filled levels well separated from two almost degenerate empty levels. Based on different DFT methods, these orbitals span the irreducible representation a_u (HOMO–1), b_{1u} (HOMO), b_{3g} (LUMO), b_{2g} (LUMO+1),[32,74,75] with some changes in the relative order of the filled and the empty levels depending on the potential. CASSCF calculations provided this order: b_{1u} (HOMO–1), a_u (HOMO), b_{3g} (LUMO), b_{2g} (LUMO+1).[76] The lowest computed dipole allowed absorptions have been reported to have $^1B_{3u}$, $^1B_{2u}$, and $^1B_{1u}$ irreducible representations both with TDDFT methods[77,78] as well as with CASPT2 calculations.[76,79] This assignment is also consistent with the Gouterman four-orbital model,[64] according to which the Q (and higher energy B) bands derive primarily from transitions from the two highest π occupied molecular orbitals into the two π^* lowest unoccupied orbitals. The spectrum, computed by us in gas phase using the SAOP potential, shows the Q-bands at 2.188 eV (B_{3u}) and 2.312 eV (B_{2u}) with oscillator strengths of 0.17×10^{-4} and 0.12×10^{-3}, polarized along the NH (3) pyrrole rings and the N pyrrole rings. The energy values are in rather good agreement with the experimental data, which fall in the range of 1.98–2.02 and 2.33–2.42,[80–82] but the splitting is too low if compared to the gas-phase measured value (0.44 eV). The same issue was reported by Baerends and co-workers[77] and was ascribed to the geometry sensitivity. Also, the values of the computed oscillator strengths are geometry-dependent and similar very small values have been reported in the literature.[78] Finally, although Q_y is commonly considered the most intense transition,[80] different computational studies identify Q_x as stronger,[78,81] in agreement with our findings. Q_x and Q_y absorptions are ascribed to HOMO–LUMO (54%) and HOMO–1-LUMO+1 (45%) and to HOMO-LUMO+1 (58%) and HOMO–1-LUMO (42%), clearly denoting the mixed character of the lowest singlet excitons, which involve the four Gouterman orbitals. This is in agreement with the analysis by Rubio and co-workers[75] and Barone *et al.*[63] We point out that no mixing of states with different orientation of transition dipole moment is present. In contrast, the lowest triplet excitons have almost monoelectronic character: for **H$_2$P**, they are computed at 1.804 eV and 2.017 eV (B_{2u}) and at 1.906 eV and 2.024 eV (B_{3u}) and are due to HOMO-LUMO+1 (96%) and HOMO–1-LUMO (96%) and to HOMO-LUMO (99%) and HOMO–1-LUMO+1 (99%).

The same analysis of the singlet and triplet lowest absorptions was carried out for **H$_2$TPPS^{4-}**, and some analogies with **H$_2$P** have emerged. The Q_y and Q_x bands are computed at 1.969 eV (B_{2u}) and at 2.502 eV (B_{3u}) with oscillator strengths of 0.0012 and 0.070, respectively. Their composition is HOMO–4-LUMO (98%) and HOMO-LUMO+1 (60%) and HOMO–5-LUMO+1 (28%). These values nicely compare to the experiment[83] and to those reported by Barone *et al.* in water.[63] Particularly, the polarization of the lowest absorptions is inverted (see Fig. 1), as amply discussed by the latter authors. The lowest triplet absorption of **H$_2$TPPS^{4-}** is computed at 1.6739 eV (B_{2u}) and corresponds to HOMO-LUMO+1 (97%) at the employed level of theory.

It is important to stress that in this work we have not put effort in optimizing the absorption wavelengths, since our primary goal is the investigation of the magnetic properties and their relation to the triplet wavefunction. As an efficient approach, we imposed D_{2h} symmetry to our systems, which very well describes **H$_2$P**, but represents only one conformer of **H$_2$TPPS^{4-}** due to the orientation of the phenyl rings, which are forced to be at 90° with respect to the porphyrin plane. Calculations of the optical properties, and in particular the polarization of the Q-bands, are relevant for the magnetophotoselection experiment, because they are employed to assign the relative orientation of the ZFS tensor axes within the molecule.

We extended the calculations to derive the ZFS parameters and the spin density distribution of the lowest triplet state of **H$_2$TPPS^{4-}**, evaluating in parallel the corresponding magnetic observables for **H$_2$P**, for which experimental and theoretical data are already available.[30,32,38] While in the main text the focus is on **H$_2$TPPS^{4-}**, the outcome of the calculations for **H$_2$P** is reported in the supplementary material.

The analysis of the frontier molecular orbitals and of the lowest excited states of **H$_2$P** and **H$_2$TPPS^{4-}** pointed out that, in both cases, a single Slater determinant description of the triplets might be nonadequate and this evidence must be taken into account when calculating the magnetic properties. Particularly, if the DFT approach gives spin density values and hyperfine tensors in nice agreement with the ENDOR experiment,[84,85] the ZFS tensor is more sensitive to the wavefunction. We started our analysis employing a DFT approach. The geometries of **H$_2$P** and **H$_2$TPPS^{4-}** were both optimized at the B3LYP-D3(BJ)/TZ2P level of theory in the triplet state. The hyperfine and ZFS tensors were also computed at the ZORA-B3LYP-D3(BJ)/TZ2Pae level as well as at the ZORA-BP86/TZ2Pae level, but no significant differences were found when comparing the results of the two approaches for **H$_2$P**.

The magnetic results were first obtained for D_{2h} constrained geometries. In order to investigate the effect of different orientations of the phenyl rings, two structures were obtained manually by imposing orientations of 30° and 60° with respect to the tetrapyrrolic plane while maintaining the geometry of the porphyrin core frozen. Importantly, the rings can be displaced in different manners and thus more conformations can be explored. We considered selected cases generated by rotating the rings clockwise (conformers A30 and A60), alternated clockwise and counterclockwise (conformers B30 and B60), and counterclockwise-clockwise-clockwise-counterclockwise (C30 and C60). Based on the energetics, the conformers with the phenyl rings rotated by 30° were discarded. The conformers with the phenyl rings rotated by 60° are the lowest energy structures, although the D_{2h} constrained geometry with the rings at 90° lies only 1 kcal mol^{-1} above. Among the 60° structures, C60 is the most stable, although by less than 0.5 kcal mol^{-1} at the employed level of theory. The hfcs of all the three conformers with the phenyl rings at 60° are found to be in excellent agreement with the experimental ENDOR data, especially for the *Z* component, which is also the most reliable direction due to the strong orientation selection that can be achieved. On the other hand, comparison with the ENDOR data provided further evidence that all the 30° conformations are unlikely to be present.

The combination of DFT calculations and ENDOR experiments allowed us to draw an accurate picture of the spin density distribution of the **H$_2$TPPS^{4-}** triplet state. Compared to the **H$_2$P** parent compound (Fig. S4), even if a small amount of spin

Author Proof

Published under license by AIP Publishing

density is moved to the phenyl rings, the overall distribution on the tetrapyrrole macrocycle is conserved.

While the values of the A tensors are in good agreement with the experiment, in the case of **H_2P** even slightly improving the results reported in the literature,[32] the computed ZFS tensor elements were unsatisfactory. Thus, we considered CASSCF as the method of choice to improve the wavefunction. For the CASSCF multiconfigurational approach, the inclusion of the whole π system of the parent **H_2P** is already computationally demanding (24 orbitals and 26 electrons), as extensively commented by Werner.[86] As the Gouterman four orbitals model has proved to be robust, we decided to define an active space formed by the four frontier orbitals, ranging from HOMO−1 to LUMO+1, which in **H_2P** as well as in **H_2TPPS^{4-}** have strong contribution from the π porphyrin core. MP2 natural orbitals were generated as guess for the CASSCF calculation. For **H_2P**, we computed two triplet states, i.e., ^3B_2u and $^3B_{3u}$, and the former was found to be more stable, in agreement with the literature. For **H_2TPPS^{4-}**, we computed ^3B_1u and $^3B_{2u}$ and the latter turned out to be more stable. The ZFS tensor was calculated using the CASSCF wavefunction, showing that the spin-orbit component is negligible, as already pointed out.

To the best of our knowledge, this is the first example of calculation of the ZFS tensor based on a CASSCF calculation for porphyrins. Further improvement might be obtained including dynamic correlation, but the multiconfigurational approach itself using the small Gouterman active space has provided good semi-quantitative results.

A number of relevant aspects about the electronic structure of the triplet state were revealed based on the comparison between **H_2TPPS^{4-}** and its parent compound **H_2P**. As a main result, while the ZFS parameters vary significantly, the ZFS tensor orientation is conserved and the triplet electron spin density distribution is found to be similar. The D parameter is about 10% smaller in **H_2TPPS^{4-}** than in **H_2P**. In contrast, the A_Z hfcs show differences of about 3%, as already pointed out in analogous comparison between the free-base tetraphenyl porphyrin and **H_2P**.[32] The excellent agreement between the experimental and calculated hfcs provides a validation of the triplet wavefunction. Calculations and experiments also agree in indicating that the presence of the sulfonate groups does not significantly alter the electronic features, as already highlighted when introducing phenyl substituents to **H_2P**.[32] This outcome is important, since the polar groups are introduced to provide solubility and should not cause unwanted variations of the electronic structure.

When comparing ZFS parameters, although they differ quite significantly in absolute values from the calculated ones, the 10% decrease in the case of **H_2TPPS^{4-}** with respect to the parent compound is also fulfilled, proving that CASSCF calculations, describing correctly the multiconfigurational nature of porphyrins, are more suitable than DFT to predict the ZFS interaction tensors. The discrepancies in the absolute values are likely due to the limited active space and to the lack of dynamic correlation. The difference in the sensitivity of the ZFS parameters and the hfcs to mesophenyl substitution finds confirmation in this work. The ZFS tensor is very sensitive, because the frontier orbitals are mainly contributing to this interaction and upon substitution part of the electron density gets slightly delocalized on the phenyl rings. Conversely, the mechanism of spin polarization governing the isotropic contribution to the hfcs derives from spin density on the core orbitals, which are unaffected by substitution effects.

In the magnetophotoselection experiments, an important aspect regarding the structural properties of **H_2TPPS^{4-}** has also emerged. As already pointed out in the Results section, the analysis of the corresponding EPR spectra has shown that the principal axes X and Y of the ZFS system are aligned along the TDM but unexpectedly the best fit has been obtained with an equal contribution of both ZFS axes, although optical excitation was performed on the main vibronic band of the Q_y transition. The apparent excitation of both Q_x and Q_y transitions with an equal contribution definitely does not match to the relative absorption of the two transitions at the excitation wavelength, and therefore, the result cannot be associated with a direct absorption process. In the quest for the mechanism that accounts for this effect, we first considered and later excluded energy transfer processes in fixed-geometry assemblies, like in the typical π-stacking aggregation. The energy transfer from one molecule to another, within the stack, and with a 90° relative rotation of the ZFS X, Y axes of two adjacent molecules, would result in the transfer of the excitation to form a distribution function that is equivalent to that generated by a pseudo Q_x-excitation. This occurrence was excluded, first because there is no excitation of any absorption band of J-aggregates at the excitation wavelength,[20] which was carefully selected to avoid any contribution; then, because both the polarization and the lineshape of the spectra did not change with concentration in diluted solutions; finally, because a population equilibration of the X and Y states is not observed experimentally.

Alternatively, a pseudorotation of the molecule may be obtained by a N–H tautomerism between two equivalent *trans* structures involving donation of the two N–H protons to the unprotonated nitrogen atoms, with the *cis* tautomer only present as a transitory intermediate.[87] We have interpreted our experimental observations invoking a fast phototautomerization process occurring in the excited singlet state, which is slowed down in the triplet state precluding its observation in the EPR time-scale. The model we have introduced to explain the magnetophotoselection experiments is represented in Fig. 5. Photoexcitation in correspondence of the Q_y band generates a distribution of the excited **H_2TPPS^{4-}** molecules with respect to the polarization of the light (see the corresponding orientational distribution function in Fig. 5) with a maximum when the molecules are oriented with the Q_y TDM parallel to the light polarization. The phototautomerization exchanges the TDM directions and also the distribution function because of the molecular pseudorotation; this is equivalent to the excitation of part of the molecules through the Q_x TDM. When singlet excitation is followed by ISC to the corresponding triplet state, the two tautomers are equivalent from the microscopic point of view, namely, the relative population rates of the three triplet sublevels are the same but their orientational distribution function is different. This is the reason why simulation of the spectra obtained by magnetophotoselection requires that both the in-plane ZFS canonical orientations are oriented along the optical polarization direction. This model accounts for the presence of two overlapping orientational distribution functions taking into account the fictitious excitation of both Q_x and Q_y bands produced by the phototautomerization in the excited singlet state. The process should be fast enough to explain the 1:1 population of the singlet excited states polarized along X and Y. At the same

AUTHOR COPY

Published under license by AIP Publishing

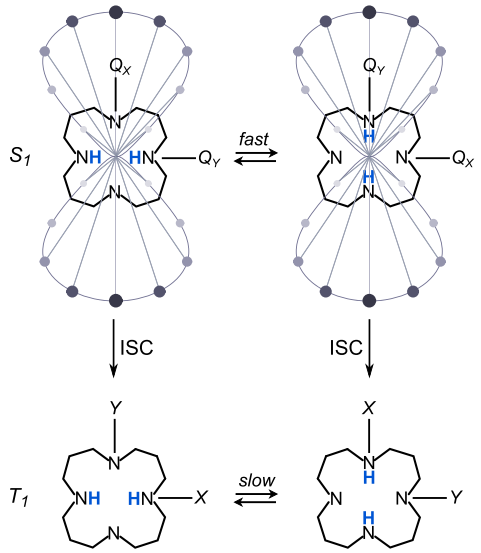

FIG. 5. Schematic representation of the photophysics and of the tautomerization process for H_2TPPS^{4-} in the excited states based on the magnetophotoselection experiments. Top: exchange of protons in the excited singlet state. The probability to excite one of the TDM directions is represented by the circles in a gray scale (with the darkest circles representing the highest probability of excitation). Bottom: ISC to the corresponding triplet state. In-plane ZFS axes are indicated.

time, a slow rate of interconversion in the triplet state accounts for the inequivalence of the *X* and *Y* transitions ($|E| \neq 0$).

Literature data support the hypothesis of a fast tautomerism in the excited singlet state for porphyrinoid molecules.[87,88] Phototautomerization of **H_2P** occurs even at cryogenic temperatures, demonstrating that it is a nonthermally activated process.[89] From the point of view of the triplet state, the process was extensively discussed for porphycenes.[90,91] EPR data are reported showing that single proton tautomerism is frozen out at low temperatures and increases as the temperature is raised and becomes visible in the EPR time-scale. Axial symmetry of the ZFS tensor has been reported for few free-base porphyrinoid model compounds, indicating fast-tautomerism also in the triplet state in these specific cases.[92,93] Free-base porphyrins show mainly rhombic symmetry ($|E| \neq 0$),[66] indicating that if tautomerization is occurring in the triplet state it is on a time scale slower than that given by the splitting of the X and Y canonical transitions. Most EPR studies of free-base porphyrins have been performed at relatively high temperatures, where thermal activation might be envisaged. Magnetophotoselection experiments, including wavelength, temperature dependence, and deuteration effects, are underway in order to clarify the complex phototautomerization behavior of this important class of molecules, which must be much slower in the triplet state as compared to the excited singlet state as highlighted in the present paper.

In conclusion, for the first time, the full characterization of the magnetic properties of H_2TPPS^{4-} was performed with an approach based on quantitative interpretation of the magnetophotoselection experiments and direct comparison of the triplet-state EPR and ENDOR data with accurate theoretical methods including CSSCF calculations of the ZFS interaction tensor. This systematic study, providing the overall picture of the triplet state and including the structural issue of tautomerization, paves the route to further triplet EPR studies on acidified and aggregated water-soluble porphyrin molecules.

SUPPLEMENTARY MATERIAL

See the supplementary material for computational details, spectral analysis of the magnetophotoselection experiments, and ^{1}H-ENDOR spectra analysis.

ACKNOWLEDGMENTS

This work was supported by the University of Padova (Grant No. PRAT 2014-CPDA145097/14). CINECA (Casalecchio di Reno, Italy) is gratefully acknowledged for providing the supercomputing facilities used for the quantum chemistry calculations through the ISCRA Grant REBEL2 (REdox state role in Bio-inspired ELementary reactions 2); P.I.: L.O. The authors thank E. Collini and C.W.M. Kay for helpful discussions and M. Dalla Tiezza and M. Bortoli for software support.

REFERENCES

[1] D. Dolphin, in *The Porphyrins*, Part B: Biochemistry (Academic Press, 1978), Vol. VII, Chap. 7.
[2] A. R. Battersby, Nat. Prod. Rep. **17**, 507 (2000).
[3] H. L. Anderson, Chem. Commun. ■, 2323 (1999). Q8
[4] J. M. Tour, Acc. Chem. Res. **33**, 791 (2000).
[5] M. O. Senge, M. Fazekas, E. G. A. Notaras, W. J. Blau, M. Zawadzka, O. B. Locos, and E. M. N. Mhuircheartaigh, Adv. Mater. **19**, 2737 (2007).
[6] J. E. Lovett, M. Hoffmann, A. Cnossen, A. T. J. Shutter, H. J. Hogben, J. E. Warren, S. I. Pascu, C. W. M. Kay, C. R. Timmel, and H. L. Anderson, J. Am. Chem. Soc. **131**, 13852 (2009).
[7] L.-L. Li and E. W.-G. Diau, Chem. Soc. Rev. **42**, 291 (2013).
[8] D. R. Ort and C. F. Yocum, *Oxygenic Photosynthesis: The Light Reactions* (Springer Netherlands, Dordrecht, 1996).
[9] L. O. Björn, G. C. Papageorgiou, R. E. Blankenship, and Govindjee, Photosynth. Res. **99**, 85 (2009).
[10] M. R. Wasielewski, Chem. Rev. **92**, 435 (1992).
[11] M. J. Llansola-Portoles, D. Gust, T. A. Moore, and A. L. Moore, C. R. Chim. **20**, 296 (2017).
[12] T. S. Balaban, Acc. Chem. Res. **38**, 612 (2005).
[13] T. Miyatake and H. Tamiaki, Coord. Chem. Rev. **254**, 2593 (2010).
[14] K. Kano, K. Fukuda, H. Wakami, R. Nishiyabu, and R. F. Pasternack, J. Am. Chem. Soc. **122**, 7494 (2000).
[15] H. J. Schneider, L. Tianjun, M. Sirish, and V. Malinovski, Tetrahedron **58**, 779 (2002).
[16] N. Micali, F. Mallamace, A. Romeo, R. Purrello, and L. Monsù Scolaro, J. Phys. Chem. B **104**, 5897 (2000).
[17] N. Micali, V. Villari, M. A. Castriciano, A. Romeo, and L. M. Scolaro, J. Phys. Chem. B **110**, 8289 (2006).
[18] E. Collini, C. Ferrante, and R. Bozio, J. Phys. Chem. B **109**, 2 (2005).
[19] A. Köhler and H. Bässler, Mater. Sci. Eng., R **66**, 71 (2009).
[20] L. Bolzonello, M. Albertini, E. Collini, and M. Di Valentin, Phys. Chem. Chem. Phys. **19**, 27173 (2017).
[21] S. Richert, C. E. Tait, and C. R. Timmel, J. Magn. Reson. **280**, 103 (2017).
[22] W. Lubitz, F. Lendzian, and R. Bittl, Acc. Chem. Res. **35**, 313 (2002).
[23] A. Toffoletti, Z. Wang, J. Zhao, M. Tommasini, and A. Barbon, Phys. Chem. Chem. Phys. **20**, 20497 (2018).
[24] D. L. Meyer, R. Matsidik, D. Fazzi, M. Sommer, and T. Biskup, J. Phys. Chem. Lett. **9**, 7026 (2018).

Author Proof

Published under license by AIP Publishing

[25] M. K. Bosch, I. I. Proskuryakov, P. Gast, and A. J. Hoff, J. Phys. Chem. **99**, 15310 (1995).
[26] W. J. McGann and H. A. Frank, Biochim. Biophys. Acta, Bioenerg. **807**, 101 (1985).
[27] C. E. Tait, P. Neuhaus, H. L. Anderson, and C. R. Timmel, J. Am. Chem. Soc. **137**, 6670 (2015).
[28] C. E. Tait, P. Neuhaus, M. D. Peeks, H. L. Anderson, and C. R. Timmel, Phys. Chem. Chem. Phys. **18**, 5275 (2016).
[29] M. Di Valentin, S. Ceola, E. Salvadori, G. Agostini, G. M. Giacometti, and D. Carbonera, Biochim. Biophys. Acta, Bioenerg. **1777**, 1355 (2008).
[30] C. W. M. Kay, M. Di Valentin, and K. Möbius, Sol. Energy Mater. Sol. Cells **38**, 111 (1995).
[31] V. Hamacher, J. Wrachtrap, B. von Maltzan, M. Plato, and K. Möbius, Appl. Magn. Reson. **4**, 297 (1993).
[32] C. W. M. Kay, J. Am. Chem. Soc. **125**, 13861 (2003).
[33] C. E. Tait, P. Neuhaus, M. D. Peeks, H. L. Anderson, and C. R. Timmel, J. Am. Chem. Soc. **137**, 8284 (2015).
[34] F. Neese, eMagRes **6**, 1 (2017).
[35] S. Sinnecker and F. Neese, J. Phys. Chem. A **110**, 12267 (2006).
[36] F. Neese, J. Chem. Phys. **127**, 164112 (2007).
[37] M. Shoji, K. Koizumi, T. Hamamoto, T. Taniguchi, R. Takeda, Y. Kitagawa, T. Kawakami, M. Okumura, S. Yamanaka, and K. Yamaguchi, *Polyhedron* (Pergamon, 2005), p. 2708.
[38] O. Loboda, I. Tunell, B. Minaev, and H. Ågren, Chem. Phys. **312**, 299 (2005).
[39] S. R. Langhoff, E. R. Davidson, M. Gouterman, W. R. Leenstra, and A. L. Kwiram, J. Chem. Phys. **62**, 169 (1975).
[40] A. Barbon, E. D. Bott, M. Brustolon, M. Fabris, B. Kahr, W. Kaminsky, P. J. Reid, S. M. Wong, K. L. Wustholz, and R. Zanré, J. Am. Chem. Soc. **131**, 11548 (2009).
[41] C. Fonseca Guerra, J. G. Snijders, G. te Velde, and E. J. Baerends, Theor. Chem. Acc. **99**, 391 (1998).
[42] G. te Velde, F. M. Bickelhaupt, E. J. Baerends, C. Fonseca Guerra, S. J. A. van Gisbergen, J. G. Snijders, and T. Ziegler, J. Comput. Chem. **22**, 931 (2001).
[43] E. J. Baerends, T. Ziegler, A. J. Atkins, J. Autschbach, D. Bashford, O. Baseggio, A. Bérces, F. M. Bickelhaupt, C. Bo, P. M. Boerritger, L. Cavallo, C. Daul, D. P. Chong, D. V Chulhai, L. Deng, R. M. Dickson, J. M. Dieterich, D. E. Ellis, M. van Faassen, A. Ghysels, A. Giammona, S. J. A. van Gisbergen, A. Goez, A. W. Götz, S. Gusarov, F. E. Harris, P. van den Hoek, Z. Hu, C. R. Jacob, H. Jacobsen, L. Jensen, L. Joubert, J. W. Kaminski, G. van Kessel, C. König, F. Kootstra, A. Kovalenko, M. Krykunov, E. van Lenthe, D. A. McCormack, A. Michalak, M. Mitoraj, S. M. Morton, J. Neugebauer, V. P. Nicu, L. Noodleman, V. P. Osinga, S. Patchkovskii, M. Pavanello, C. A. Peeples, P. H. T. Philipsen, D. Post, C. C. Pye, H. Ramanantoanina, P. Ramos, W. Ravenek, J. I. Rodríguez, P. Ros, R. Rüger, P. R. T. Schipper, D. Schlüns, H. van Schoot, G. Schreckenbach, J. S. Seldenthuis, M. Seth, J. G. Snijders, S. M. ■, M. Solà, M. Swart, D. Swerhone, G. te Velde, V. Tognetti, P. Vernooijs, L. Versluis, L. Visscher, O. Visser, F. Wang, T. A. Wesolowski, E. M. van Wezenbeek, G. Wiesenekker, S. K. Wolff, T. K. Woo, and A. L. Yakovlev (2018).
[44] A. D. Becke, J. Chem. Phys. **98**, 5648 (1993).
[45] C. Lee, W. Yang, and R. G. Parr, Phys. Rev. B **37**, 785 (1988).
[46] S. H. Vosko, L. Wilk, and M. Nusair, Can. J. Phys. **58**, 1200 (1980).
[47] S. Grimme, S. Ehrlich, and L. Goerigk, J. Comput. Chem. **32**, 1456 (2011).
[48] O. V. Gritsenko, P. R. T. Schipper, and E. J. Baerends, Chem. Phys. Lett. **302**, 199 (1999).
[49] P. R. T. Schipper, O. V. Gritsenko, S. J. A. van Gisbergen, and E. J. Baerends, J. Chem. Phys. **112**, 1344 (2000).
[50] L. Orian, S. Scuppa, S. Santi, and M. Meneghetti, Phys. Chem. Chem. Phys. **15**, 12971 (2013).
[51] S. Scuppa, L. Orian, D. Dini, S. Santi, and M. Meneghetti, J. Phys. Chem. A **113**, 9286 (2009).
[52] S. Scuppa, L. Orian, A. Donoli, S. Santi, and M. Meneghetti, J. Phys. Chem. A **115**, 8344 (2011).
[53] A. D. Becke, Phys. Rev. A **38**, 3098 (1988).
[54] J. P. Perdew, Phys. Rev. B **33**, 8822 (1986).
[55] J. P. Perdew, Phys. Rev. B **34**, 7406 (1986).
[56] E. van Lenthe, E. J. Baerends, and J. G. Snijders, J. Chem. Phys. **99**, 4597 (1993).
[57] R. van Leeuwen, E. van Lenthe, E. J. Baerends, and J. G. Snijders, J. Chem. Phys. **101**, 1272 (1994).
[58] E. van Lenthe, J. Chem. Phys. **110**, 8943 (1999).
[59] F. Neese, Wiley Interdiscip. Rev.: Comput. Mol. Sci. **2**, 73 (2012).
[60] I. V. Borovykh, I. B. Klenina, I. I. Proskuryakov, P. Gast, and A. J. Hoff, in *Spectroscopy of Biological Molecules: New Directions* (Springer Netherlands, Dordrecht, 1999), pp. 189–190.
[61] A. Regev, S. Michaeli, H. Levanon, M. Cyr, and J. L. Sessler, J. Phys. Chem. **95**, 9121 (1991).
[62] L. Giovanelli, H.-L. Lee, C. Lacaze-Dufaure, M. Koudia, S. Clair, Y.-P. Lin, Y. Ksari, J.-M. Themlin, M. Abel, and A. A. Cafolla, J. Electron Spectrosc. Relat. Phenom. **218**, 40 (2017).
[63] R. Improta, C. Ferrante, R. Bozio, and V. Barone, Phys. Chem. Chem. Phys. **11**, 4664 (2009).
[64] M. Gouterman, J. Mol. Spectrosc. **6**, 138 (1961).
[65] J. R. Lakowicz, *Principles of Fluorescence Spectroscopy* (■, 2006).
[66] J. H. van der Waals, W. G. van Dorp, and T. J. Schaafsma, in *Porphyrins*, edited by D. Dolphin (Academic Press, 1979), Vol. IV, pp. 257–312.
[67] E. Salvadori, M. Di Valentin, C. W. M. Kay, A. Pedone, V. Barone, and D. Carbonera, Phys. Chem. Chem. Phys. **14**, 12238 (2012).
[68] This conformer was also optimized maintaining the core frozen and the phenyl rings rotated until they reached the dihedral values of 60 degrees with respect to the tetrapyrrolic plane., (n.d.).
[69] W. A. J. A. van der Poel and J. H. van der Waals, Mol. Phys. **53**, 673 (1984).
[70] W. G. van Dorp, M. Soma, J. A. Kooter, and J. H. van der Waals, Mol. Phys. **28**, 1551 (1974).
[71] A. Kawai, T. Hidemori, and K. Shibuya, *Molecular Physics* (Taylor & Francis Group, 2006), pp. 1573–1579.
[72] S. Michaeli, S. Soffer, H. Levanon, M. O. Senge, and W. W. Kalish, J. Phys. Chem. A **103**, 1950 (1999).
[73] D. Carbonera, M. Di Valentin, R. Spezia, and A. Mezzetti, Curr. Protein Pept. Sci. **15**, 332 (2014).
[74] D. Lamoen and M. Parrinello, Chem. Phys. Lett. **248**, 309 (1996).
[75] M. Palummo, C. Hogan, F. Sottile, P. Bagalá, and A. Rubio, J. Chem. Phys. **131**, 084102 (2009).
[76] M. Merchán, E. Ortí, and B. O. Roos, Chem. Phys. Lett. **226**, 27 (1994).
[77] S. J. A. van Gisbergen, A. Rosa, G. Ricciardi, and E. J. Baerends, J. Chem. Phys. **111**, 2499 (1999).
[78] D. Sundholm, Phys. Chem. Chem. Phys. **2**, 2275 (2000).
[79] L. Serrano-Andrés, M. Merchán, M. Rubio, and B. O. Roos, Chem. Phys. Lett. **295**, 195 (1998).
[80] L. Edwards, D. H. Dolphin, M. Gouterman, and A. D. Adler, J. Mol. Spectrosc. **38**, 16 (1971).
[81] B. F. Kim and J. Bohandy, J. Mol. Spectrosc. **73**, 332 (1978).
[82] U. Nagashima, T. Takada, and K. Ohno, J. Chem. Phys. **85**, 4524 (1986).
[83] D. L. Akins, H. R. Zhu, and C. Guo, J. Phys. Chem. **100**, 5420 (1996).
[84] M. Di Valentin, C. E. Tait, E. Salvadori, L. Orian, A. Polimeno, and D. Carbonera, Biochim. Biophys. Acta, Bioenerg. **1837**, 85 (2014).
[85] A. Agostini, M. G. Dal Farra, H. Paulsen, A. Polimeno, L. Orian, M. Di Valentin, and D. Carbonera, J. Phys. Chem. B **123**, 8232 (2019).
[86] P. Celani and H.-J. Werner, J. Chem. Phys. **112**, 5546 (2000).
[87] J. Waluk, Acta Phys. Pol., A **95**, 49 (1999).
[88] M. Stępień and L. Latos-Grażyński, *Aromaticity in Heterocyclic Compounds* (Springer Berlin Heidelberg, Berlin, Heidelberg, 2008), pp. 83–153.
[89] S. Völker and J. H. van der Waals, Mol. Phys. **32**, 1703 (1976).
[90] C. W. M. Kay, G. Elger, and K. Möbius, Phys. Chem. Chem. Phys. **1**, 3999 (1999).
[91] C. W. M. Kay, U. Gromadecki, J. T. Törring, and S. Weber, Mol. Phys. **99**, 1413 (2001).
[92] P. J. Angiolillo and J. M. Vanderkooi, Biophys. J. **68**, 2505 (1995).
[93] H. Levanon, A. Regev, T. Galili, M. Hugerat, C. K. Chang, and J. Fajer, J. Phys. Chem. **97**, 13198 (1993).

Author Proof

Published under license by AIP Publishing